Engineering Applications of Computational Fluid Mechanics Vol.8, No.1, pp. 140-157 (2014)

RESEARCH ON RUNNING STABILITY OF CRH3 HIGH SPEED TRAINS PASSING BY EACH OTHER

Zhenxu Sun*, Yingying Zhang, Dilong Guo, Guowei Yang and Yubiao Liu

Key laboratory for Mechanics in Fluid Solid Coupling Systems, Institute of Mechanics, Chinese Academy of Sciences, Beijing 100190, China
*E-Mail: sunzhenxu@imech.ac.cn (Corresponding Author)

ABSTRACT: Two scenarios of trains passing by each other are usually encountered, which are trains passing by each other in the tunnel and passing by each other in the open air, respectively. The prototype of the CRH3 high speed train is considered in the present paper, with bogies, windshields, pantograph shrouds, air conditioner shrouds and other complex structures taking into consideration. Aerodynamic loads and multi-body system response of this prototype are discussed under the conditions of both scenarios. The variations of aerodynamic loads and the pressure on the surface of the trains are mainly analyzed, and then the formation mechanism of the variations is discussed. A comparative study of the differences in both scenarios is also performed. In addition, the dynamic response of the high speed train has been studied by loading the unsteady aerodynamic forces and torques. Furthermore, the derailment coefficient, the wheel unloading rate, the wheel/rail lateral force and the wheel/rail vertical force are analyzed as assessment criteria to verify the running stability in the two scenarios. The most unsafe position during the process of trains passing by each other and the variation of the four parameters with the speed is obtained. Then the linear fit between the four parameters and the speed has been performed, and the limiting speed under these two scenarios are also obtained. As a result, the results of this paper could provide guidance for safe running of trains passing by each other in reality.

Keywords: aerodynamic loads, tunnel pressure waves, multi-body dynamic analysis, running stability

1. INTRODUCTION

The development of high-speed train necessitates the corresponding advancement in technology. In recent years, China's high-speed train technology has made significant progress. The operating speed of Beijing-Shanghai high-speed rail has been up to 300 km h-1. In the case of high-speed operation, the aerodynamic characteristics of high-speed trains become more complex, since high-speed trains run close to the ground and their aspect ratio is much larger than other ground vehicles (Raghuathan et al., 2002; Baker, 2010; Tian, 2009). With the increase of the running speed, a series of problems associated with safety of running trains emerge and even lead to greater traffic accidents, resulting in huge economic losses. The dynamic characteristics of the train have been an important aspect of vehicle design. Plenty of research has been done on the train-rail system and the structural design of the train, but the research on train vibration problems due to aerodynamic excitations could hardly be found because this phenomenon is not prominent when trains run at low speeds. However, as the running speed increases, more attention should be paid to multi-body dynamics problems triggered by aerodynamic excitations and related safety issues.

Within all the running scenarios, the scenarios of a train running under the crosswind condition and trains passing by each other in a tunnel or in the open air have a relatively larger impact on the running safety of trains. Under the crosswind conditions, large separation vortices in the leeward side of a train would emerge, and the train has to withstand great lateral force and overturning moment. These could easily result in derailment and rollover of train. The research on the running safety of trains under the crosswind condition is relatively mature and the derailment coefficient and the wheel unloading rate can easily be obtained (Mao et al., 2011), since the numerical simulation of trains in the crosswind condition does not require the moving mesh technique and the aerodynamic loads of each car of the train can be computed precisely by CFD (Hemida and Krajnovic, 2008 and 2010; Baker et al., 2011). Strong pressure waves will arise when two trains pass by each other. The pressure waves are a kind of instantaneous pressure shock phenomenon, resulting in a strong disturbance to the surrounding air and a drastic change of pressure on the surface of the train. It would affect badly the running safety and amenity. The running safety problem when trains pass by each other has become one of the limiting factors to the

Received: 5 Nov. 2012; Revised: 31 Oct. 2013; Accepted: 25 Nov. 2013

further increase of the speed of high-speed trains. In recent years, due to gradually increasing attention to pressure wave characteristics and the safety problems of high speed trains, a large number of studies have been carried out in China and other countries using experiments and numerical simulations. The early study on trains passing by each other mainly focused on the surface pressure of the train and the aerodynamic loads acting on the train body, which were studied with the boundary element or finite difference numerical method by solving the Euler or NS equations (Katsuhiro et al., 1996; Hwang et al., 2001). Experimental study of the pressure waves was carried out, for example by Robert et al. (2002) and Liang and Tian (2002). When trains pass by each other in a tunnel, strong transient pressure impulses will emerge on the surface of the trains and the tunnel wall. The research on this process is of great significance to optimize the design of the trains and the facilities around tunnels, to reduce aerodynamic noise pollution and to improve the train comfort and safety. Due to the particularity of this problem, the research is generally performed through dynamic model tests and CFD numerical simulations. The flow field is rather complicated when trains pass by each other in a tunnel because of the following reasons: a) the flow is three-dimensional, compressible, unsteady and turbulent; b) relative motion exists between the tunnel and the trains, and also between the two trains, which could not be calculated by traditional numerical methods; c) compared to the tunnel, the scale of the components of the train is relatively small, which would impose great difficulties for mesh generation.

However, publications on multi-body dynamic response analysis and the corresponding safety problem could be found for trains passing by each other. There are two reasons for this. First, it is more difficult to predict the aerodynamic loads precisely. Compared to the scenario that a train runs in the open air or in the crosswind condition, numerical simulation of trains passing by each other needs moving mesh to simulate the relative movement between the trains. It is difficult to consider all the auxiliary parts of the train when calculating two trains at the same time. Traditional studies mainly focus on the time history of tunnel compressible or expansion waves. The pressure waves are mainly affected by the shape of the train and the blockage ratio between the train and tunnel. As a result, the auxiliary components of the train could be neglected, and a simplified model could be adopted. However, when it comes to train aerodynamic calculation, the influence of the subsidiary components on aerodynamic forces is obvious and their effects must be taken into account, imposing a challenge to large scale calculation based on a moving mesh. Second, for the multi-body system response analysis, the aerodynamic forces and torques based on the centroid of each car should be loaded. In these conditions, the centroid of each car moves together with the train and the aerodynamic forces also have obvious unsteady characteristics. Therefore, the aerodynamic loads need to be converted based on the time-varying centroid of each car.

In this paper, the analysis of aerodynamic characteristics and the running safety of trains passing by each other in the open air and in a tunnel has been performed with the use of the moving mesh technique. The unsteady aerodynamic load characteristics of the train under both scenarios and the dynamic response of the train under unsteady aerodynamic loads are both under investigation. In order to provide guidance for the running safety in reality, the dynamic response of the train at different speeds is also analyzed. Limiting speed of trains can be obtained by analyzing the derailment coefficient, the wheel unloading rate, the wheel/rail lateral force and the wheel/rail vertical force, and safety performance of the train in both scenarios is also compared.

2. ALGORITHMS

2.1 Moving mesh technique

The relative motion between trains need to be considered in the present paper. Traditional CFD methods assume the reference coordinate system is placed on the train body and uniform flow is imposed on the inlet of the computational domain, which is not suitable for the present study. Taking into account the characteristics of running trains, the sliding mesh should be adopted, and the dynamic layering method is used in the running direction of the train.

The sliding mesh method (Sanjay, 1994) meshes computational domains of both moving and stationary objects and non-continuous grids could be used at the interface. With the translation of the moving region, boundary mesh of different regions slips with each other at the interface. Interpolation of variables is used at the interface, and the flux on both sides is continuous. But only relying on the sliding mesh for translation, the

mesh will be intertwined, and the corresponding boundary will change subsequently. Thus, it must be combined with the dynamic layering method. The dynamic layering method could be used to add or remove layers of cells adjacent to a moving boundary, based on the height of the layer adjacent to the moving surface.

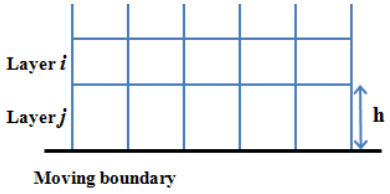

Fig. 1 Schematic of dynamic layering method.

As shown in Fig.1, if the boundary is moving upward, the cells in the j-th layer will be compressed until $h < \alpha_c h_{ideal}$, where $\alpha_c (0 < \alpha_c < 1)$ is the combined coefficient and and h_{ideal} is the ideal cell height. Then the cells in the j-th and i-th layer will be combined together. If the boundary is moving downward, the cell heights are allowed to increase until $h > (1+\alpha_s)h_{ideal}$, where $\alpha_s (0 < \alpha_s < 1)$ is the splitting coefficient. When this condition is met, the cells are split based on the specified layering option: constant height or constant ratio. Details of the moving mesh technique could be found in literature (Fluent Inc., FLUENT 6.3 User's Guide).

2.2 Turbulent models

The unsteady RANS approach has been adopted to solve the flow field when trains pass by each other. URANS solves classic RANS by unsteady method, based on the time average, phase average and fluctuating values of physical quantity associated with the time in the flow field (Nishino et al., 2008; Hussain and Reynolds, 1970), even the boundary conditions are constant (Spalart, 2000). The primary transport variables are governed by conservation equations of mass and momentum:

$$\frac{\partial \rho}{\partial t} + \nabla \cdot (\rho \vec{v}) = 0 \tag{1}$$

$$\frac{\partial}{\partial t}(\rho \vec{v}) + \nabla \cdot (\rho \vec{v}\vec{v}) = -\nabla p + \nabla \cdot (\mu \nabla \vec{v}) + \vec{S}_M \tag{2}$$

where $\vec{S}_M$ is the source term, which could be expressed as:

$$\vec{S}_M = \rho \vec{g} + \frac{\partial}{\partial x_i}\left(\mu \frac{\partial \nu_i}{\partial x_j}\right)\vec{e}_j - \frac{2}{3}\nabla(\mu \nabla \cdot \vec{\nu}) \tag{3}$$

The fluctuating values lead to the emergence of Reynolds stress terms in the Reynolds-averaged equations. Turbulence model needs to be introduced to close the equations in order to solve each physical quantity in the flow field. The realizable $k-\varepsilon$ turbulence model is adopted (Spalart, 2000), which evolves on the basis of the standard $k-\varepsilon$ model and satisfies the Reynolds stress constraints. This model has more advantages in solving flows with large separations and larger adverse pressure gradients. This model is a two-equation model, with two additional transport equations for turbulent kinetic energy k and turbulent dissipation rate ε, as follows.

$$\frac{\partial}{\partial t}(\rho k) + \frac{\partial}{\partial x_j}(\rho k v_j) = \frac{\partial}{\partial x_j}\left[\left(\mu + \frac{\mu_t}{\sigma_k}\right)\frac{\partial k}{\partial x_j}\right] + G_k + G_b - \rho\varepsilon - Y_M \tag{4}$$

$$\frac{\partial}{\partial t}(\rho \varepsilon) + \frac{\partial}{\partial x_j}(\rho \varepsilon v_j) = \frac{\partial}{\partial x_j}\left[\left(\mu + \frac{\mu_t}{\sigma_\varepsilon}\right)\frac{\partial \varepsilon}{\partial x_j}\right] + \rho C_1 S\varepsilon - \rho C_2 \frac{\varepsilon^2}{k + \sqrt{\nu\varepsilon}} + C_{1ò}\frac{\varepsilon}{k}C_{3\varepsilon}G_b \tag{5}$$

The expressions for the variables in the above equations could be found in the literature (Shih et al., 1995) and will not be listed in the present paper for simplicity. When solving the above equations, the SIMPLE algorithm has been adopted to deal with the pressure-velocity coupling problem, while the second order upwind discritization has been used for the momentum, k and ε equations.

2.3 Multi-body dynamic model

In the coupling process of the train with the air flow, the train body is the main object that the flow is around, and the elastic deformation of the train body is relatively small, compared to the geometry of its own. Therefore, during the dynamic response analysis of the train system, the elastic deformation has been ignored and the various components of the train system are considered as rigid bodies. The equation for the dynamic response analysis of the train system can be established using Lagrange principle, and can be expressed in the following unified form:

$$M\ddot{X} + F(\dot{X}, X) = F_r + F_a \tag{6}$$

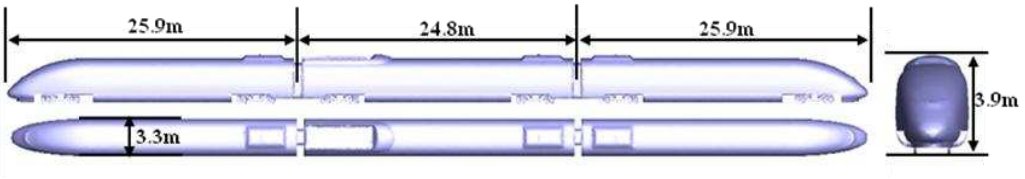

Fig. 2 Computational model.

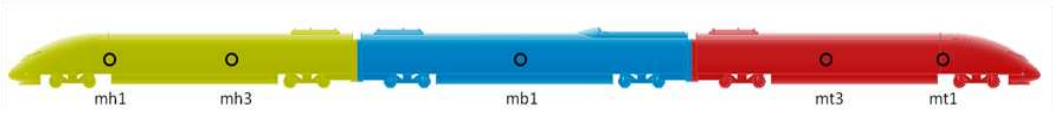

Fig. 3 Locations of test points.

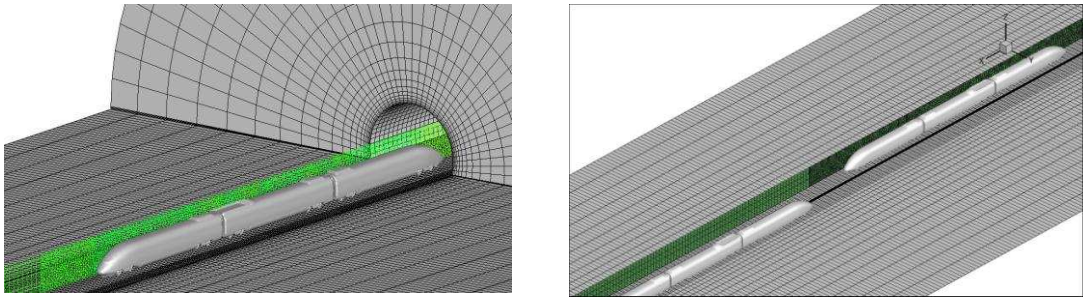

(a) Grids for trains passing by each other in the tunnel

(b) Grids for trains passing by each other in the open air

Fig.4 Computational grids.

in which M is mass matrix; X, $\dot{X}$ and $\ddot{X}$ are the generalized displacement vector, the generalized velocity vector, and the generalized acceleration vector, respectively; F_r is the generalized vector of the track excitations, with Beijing-Tianjin-track spectrum adopted in this paper; F_a is the aerodynamic loads; $F(\dot{X}, X)$ is the generalized vector including the suspension force, the connected devices force and the wheel-track force.

3. COMPUTATIONAL MODEL AND CONDITIONS

The analysis of aerodynamic loads and running safety of the CRH3 high speed trains passing by each other in a tunnel and in the open air has been performed. In order to accurately predict aerodynamic loads of the train, the computational model should be as realistic as possible and includes the windshields, bogies, air conditioner shrouds, pantograph shroud and other subsidiary structures. Fig.2 shows the computational model used in this paper.

The tunnel used for trains passing by each other is a double-track tunnel, with a cross-sectional area 100 ㎡ and length 390m. Since the pressure waves in the tunnel can be reflected many times during the trains travel through the tunnel, the impact of the pressure waves on the aerodynamic loads of the train can be fully considered. In order to record the pressure variation, test points are placed in different parts of the train body. The locations of the test points are shown in Fig. 3. Multiple blocks have been adopted for mesh generation. Two cuboid zones have been used as the moving zone for each train, and the structural grids have been utilized for the outside stationary zone. The relative movement between different blocks has been achieved by the sliding mesh technique and the dynamic layering method has been adopted to maintain the invariance of the computational domain. Fig.4 shows the grids for trains passing by each other in the tunnel and in the open air.

Hybrid mesh is adopted for the mesh generation in the moving zones. The core area around the train uses unstructured grids, while the region near the wall uses prism grids to capture the flow detail within the boundary layer. The y+ along the surface of the train ranges from 30-100 to ensure the use of wall functions. Structured grids are generated outside the core region for mesh

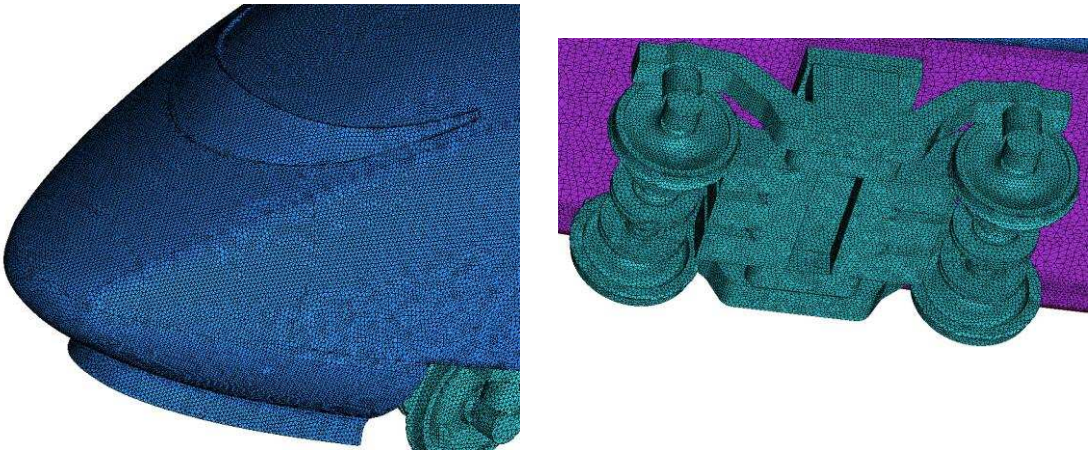

(a) Streamline (b) First bogie

Fig.5 Typical mesh distributions around surface of train.

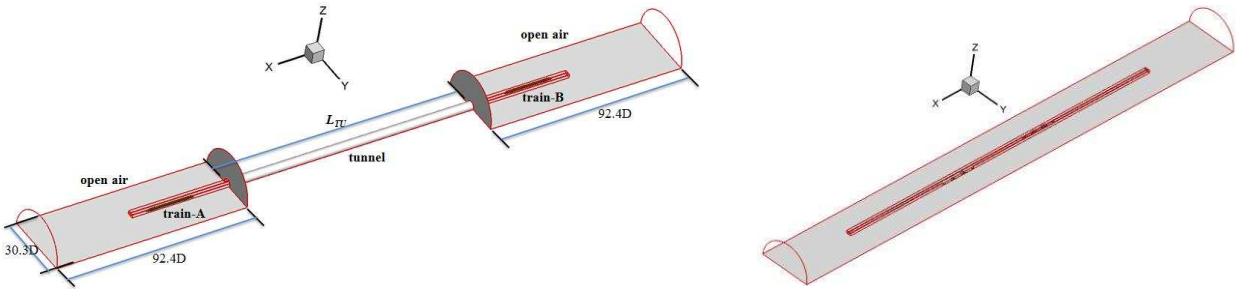

(a) Trains passing by each other in tunnel (b) Trains passing by each other in open air

Fig.6 Whole computational domain.

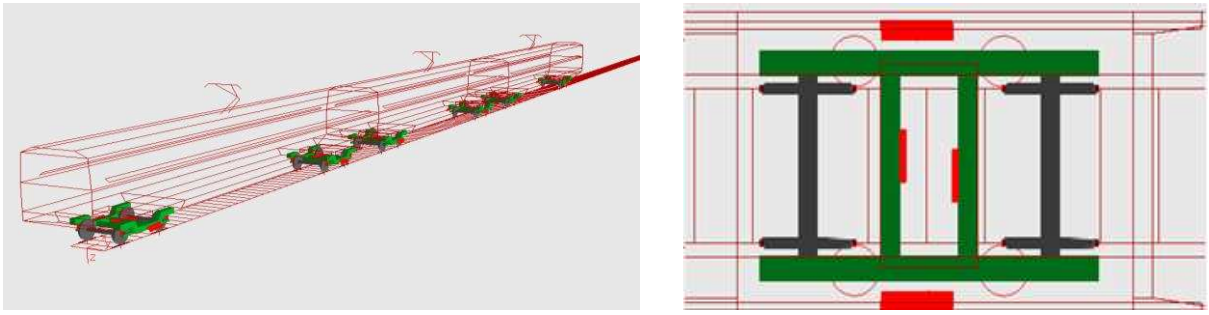

(a) Whole train (b) Wheelsets and bogie frame

Fig.7 Model for multi-body analysis.

updating. The total number of the grids is around 12 million. Typical mesh distributions around the surface of the train are shown in Fig. 5.

Denoting D the width of the high speed train, the lengths of the domain before and after the tunnel are both set as 92.4D, the width of the domain is set as 30.3D, and the length of the tunnel is L_{TU}=118.2D. The whole domain for trains passing by each other in a tunnel is shown in Fig. 6a.

For trains passing by each other in the open air, the computational domain is almost the same as in Fig. 6, except that the tunnel is eliminated and the region outside the tunnel is included as computational domain, which is shown in Fig. 6b. The ambient air could be greatly compressed when trains passing by each other, so the compressibility of air in the calculations needs to be considered and the flow field should be solved by compressible NS equations. Since the reference coordinate system is set on the ground, the trains wall, tunnel wall and the ground are all set as no-slip wall conditions. The far field of the

Table 1 Computational cases.

Scenarios	Running speeds (km/h)
Trains passing by each other in tunnel	250、300、350、400
Trains passing by each other in open air	250、300、350、400

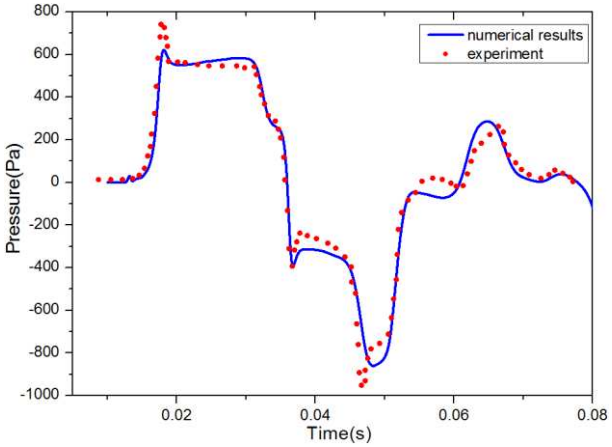

Fig.8 Comparisons between experimental and numerical data at l=900mm.

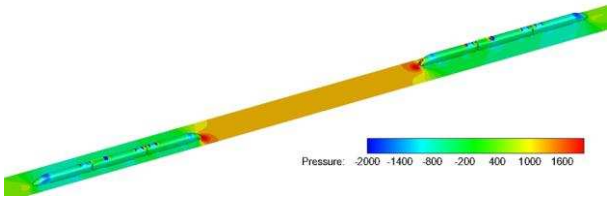

(a) Typical pressure contour

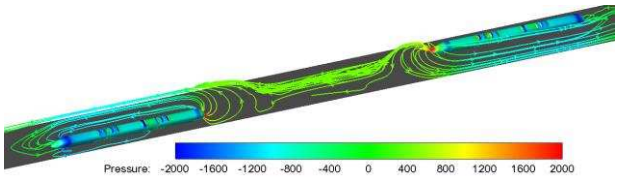

(b) Streamlines

Fig.9 Typical pressure contour and streamlines when trains pass by each other in tunnel.

domain uses pressure outlet condition, and the far-field pressure is set as 1atm. The zones which the trains belong to are assumed as moving domains, with its speed the same as the train.

Similar to the flow analysis, the model used for multi-body analysis is also a three-carriage model, comprising the leading car, the middle car and the trailing car. Ignoring the elastic deformation, the train system is assumed as a multiple rigid body system connected with a variety of flexible suspension components. The model for multi-body analysis is shown in Fig. 7.

In order to study the response characteristics under different running speeds, several speeds have been considered in the present paper. All computational cases are shown in Table 1.

4. RESULTS AND DISCUSSIONS

4.1 Numerical validation

In this section the experiments in literature (Pierre et al., 2007) are taken as the test case for numerical validation. The experiments were conducted at the von Karman Institute for Fluid Dynamics. The tunnel is 6-meter long with a uniform circular cylindrical section of 99mm in diameter. The long train model which is 600mm in length and 38mm in diameter is adopted for validation. It has a conical nose with an angle of 60° between the axis and the directrix. Numerical models and computational conditions are the same as the experimental ones. The running speed of the train is chosen as 140 km/h. An axisymmetrical computation has been performed with the same algorithms proposed in the present paper. A typical pressure pattern is obtained for the probe at l=900mm from the tunnel extrance, which is shown in Fig. 8 together with the experimental results.

As seen in Fig. 8, the numerical results agree well with the experimental results, indicating that the algorithms proposed in the present paper could be used for further study.

4.2 Analysis of aerodynamic characteristics

Aerodynamic loads are the root of the multi-body system response of high speed trains, and the analysis of aerodynamic forces can effectively predict multi-body response characteristics of the train. Therefore, before conducting safety analysis, this paper first analyzes aerodynamic characteristics in different scenarios and studies the unsteady variation, then the aerodynamic forces and torques are loaded on the multi-body dynamics model and the multi-body response characteristics of the train are then analyzed.

4.2.1 Trains passing by each other in tunnel

When the trains pass by each other in the tunnel, the aerodynamic loads get distinct features. There exist bidirectional compression and expansion waves in the tunnel, and the combined effects of both will affect aerodynamic loads of the train. Trains passing by each other in the limited space

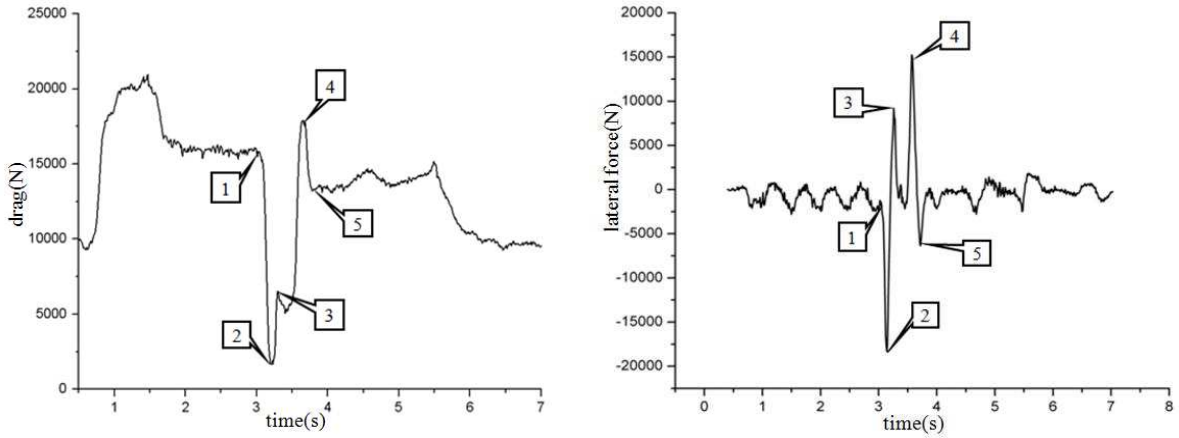

(a) Aerodynamic drag on leading car (b) Lateral force on leading car

Fig.10 Time history of aerodynamic drag and lateral force on leading car.

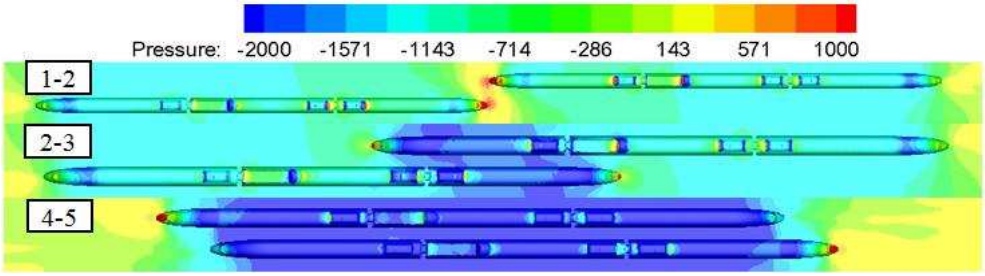

Fig.11 Pressure contours for different characteristic time periods during trains passing by each other.

will cause sudden changes of the circulation area of the airflow around the train, and thus cause the change of the resistance characteristics. Fig. 9 shows the typical pressure contour and streamlines of trains passing by each other at the speed of 300km/h in the tunnel.

It can be seen that the positive pressure in front of the nose of the leading car is constantly imposed before the trains passing by each other, and this leads to larger aerodynamic drag on the train. As seen in Fig. 9b, the flow accelerates from the leading nose, propagates backward on both sides of the train and merge on the trailing nose. Confined by the tunnel surface, the speed of the flow when passing by the middle part of the train gets higher, resulting in relatively low pressure there. Due to the asymmetrical space on the lateral sides of the train, the magnitude of the lateral force gets considerably larger, while the flow in the middle of both trains gets rather turbuluent.

Taking the aerodynamic loads the leading car withstands at the speed of 300km/h for example. Fig. 10 shows the aerodynamic drag and lateral force of the leading car.

In order to facilitate the analysis, the relative positions of the trains in each characteristic time period, as well as the corresponding pressure contours, are shown in Fig. 11.

As seen in Fig. 10a, when the trains run into the tunnel, the drag on the leading car substantially increases due to the extrusion of the tunnel wall. Compared with the single train passing through the tunnel, the drag on the trains passing by each other increases more prominently, with an increase of 115% in amplitude. After the trains totally run into the tunnel, a stable period of the drag on the leading car could be observed, but this steady value is still about 71% higher relative to the drag on the train running in the open air. However, when two trains are passing by each other, the drag changes greatly. Different from the drag characteristics of trains passing by each other in the open air, the drag on the leading car during trains passing by each other in the tunnel drastically reduces, because the airflow circulation area plunges in the tunnel at the meeting moment and the surrounding air flow speed is significantly improved, resulting in a sudden drop of pressure. As seen in Fig. 11, during the process that the trains pass by each other, the region around the train body is always surrounded by low pressure due to the narrow sectional area, thus the overall drag on the train

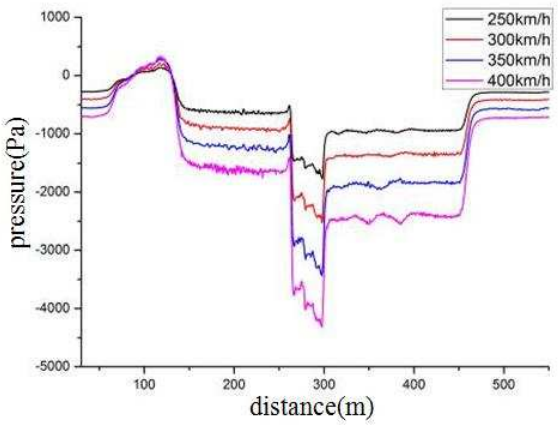

Fig.12 Pressure variation at mh1 under different speeds.

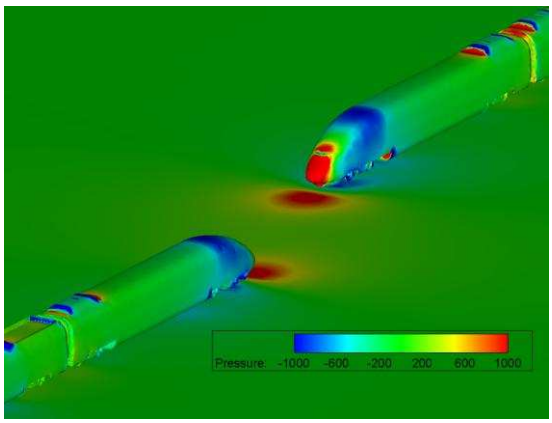

(a) Typical pressure contour

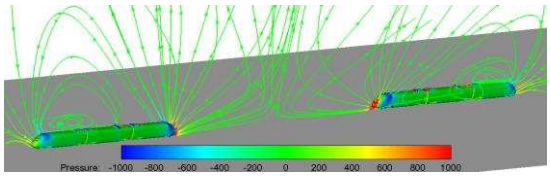

(b) Typical streamlines

Fig.13 Typical pressure contour and streamlines for trains passing by each other in open air.

reduces at this time. At point of time No. 2 in Fig. 10a, the local drag that the leading car bears reaches a minimum value. This value is even lower than on the train running in the open air, only 18% of its amplitude. This phenomenon could only be seen when trains pass by each other in the tunnel and could not be observed for trains passing by each other in the open air.

As seen in Fig. 10b, the evolution of lateral force is mainly affected by the pressure distribution on the leading and trailing streamlines. In order to facilitate the description, the train under analysis is named train-A, and the opposite train is named train-B. Before the trains pass by each other, the positive pressure zone on the streamline of train-B could directly affect the streamline of train-A, and greatly increases the lateral force. After the streamlines pass by each other, the negative pressure just behind the streamline begins to be predominant. Consequently, the lateral force on train-A begins to decrease, and even reverses. Before the leading car of train-A runs into the stagnation zone around the trailing nose cone of train-B, the suction controlled by the low pressure is dominant. After running into the stagnation zone, the suction reduces due to the influence of higher pressure there, and then the lateral force also becomes gradually smaller.

The pressure history at test point mh1 on the leading car of train-A at different speeds is shown in Fig.12.

Relatively strong negative pressure could be observed in Fig. 12, which is consistent with the time when the minimum of the drag occurs. Observing the maximum and the minimum pressure of all test points at different speeds, the pressure extremums are approximately +225.75Pa/-1854.1Pa when the train runs at the speed of 250km/h; the pressure extremums are approximately +576.16Pa/-4632.37Pa at the speed of 400km/h, which are 255.2% and 249.8% of the extremums respectively at the speed of 250km/h. As can be seen, the running speed has a significant impact on the amplitude of pressure waves generated when trains pass by each other. Relationships between the pressure extremums and the running speed could be obtained through numerical fitting: $P_{max} = 0.05625V_{train}^{1.9619}$ and $P_{min} = -0.44906V_{train}^{1.962}$, with correlation coefficient of 0.998 and 0.999, respectively. It can be seen that the pressure extremums generated by trains passing by each other in the tunnel are proportional to the square of the speed.

4.2.2 Trains passing by each other in open air

No walls exist outside the trains in the present case, so the pressure waves could not be reflected when trains pass by each other. The airflow around the trains will not be constrained in a limited space, so that the airflow circulation space will not drop drastically. Aerodynamic loads in the present case are mainly influenced by the pressure distribution around the leading and trailing streamline of the opposite train. Typical pressure contour and spatial streamlines of the train body are shown in Fig. 13. The air will decelerate when flowing close to the nose of the leading car, then stagnate at the nose of the leading car where a high pressure zone exists.

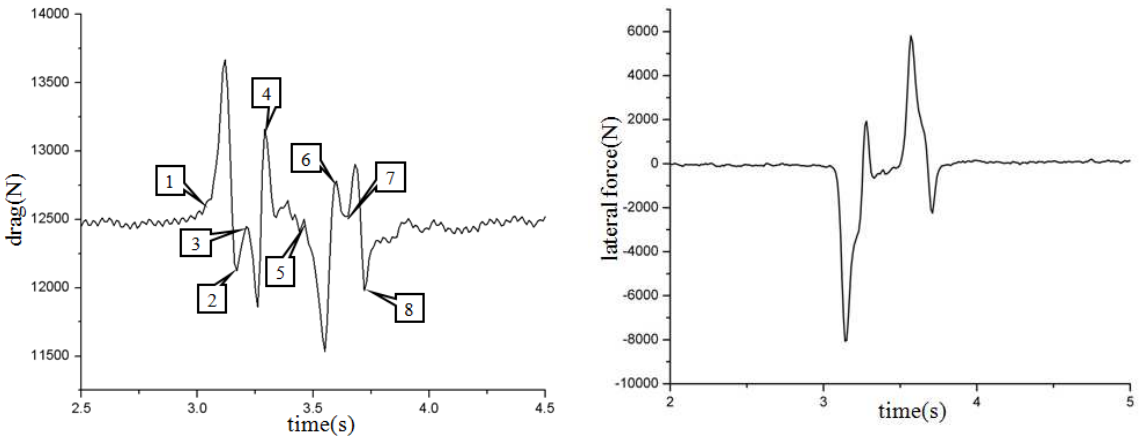

(a) Aerodynamic drag (b) Lateral force

Fig.14 Time history of aerodynamic drag and lateral force on leading car.

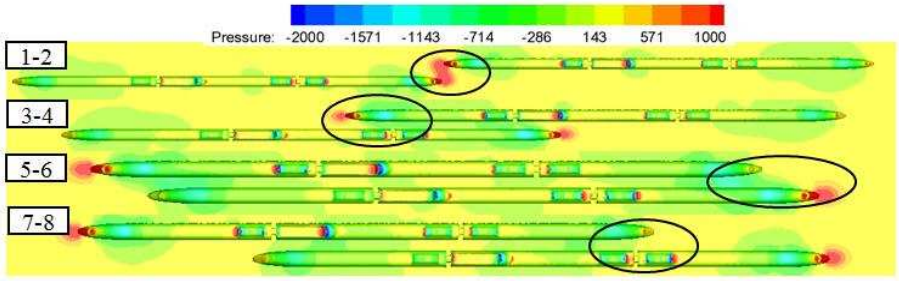

Fig.15 Pressure contours for different characteristic time periods during trains passing by each other.

When the flow passes along the streamline, its velocity gets increased and a low pressure zone will be generated. Pressure distribution near the trailing streamline is similar to that of the leading streamline, although the amplitude of the high-pressure zone is far lower than that of the leading streamline. Different from the scenario that trains pass by in the tunnel, the flow gets less disturbed when trains pass by each other in the open air and enough space is available for the compressed flow to propagate outward. As a result, the disturbance to the train by the flow is a little weaker, which could be reflected from the aerodynamic loads acting on the train.

The evolution of the aerodynamic drag and lateral force which the leading car withstands at the speed of 300km/s is given in Fig. 14.

The positions where the drag changes drastically have been marked out in Fig. 14a. Specific positions and corresponding pressure distributions are shown in Fig. 15.

It can be seen that the drag on the leading car is mainly affected by the pressure distribution of the leading and trailing streamline of the opposite train. Fig. 15 gives four typical time periods of the trains passing by each other. When the high pressure region of the opposite train influences mainly the upstream zone of the leading car, the drag on the leading car will increase, and vice versa. When the low pressure region of the opposite train influences mainly the upstream zone of the leading car, the drag will decrease, and vice versa. The drag on the leading car of each time period in Fig. 15 is not monotonic, which is a consequence of the presence of the high pressure zone and the low pressure zone near the streamline.

Similarly the pressure distribution around the streamline will also affect lateral forces. When passing through the positive pressure zone of the opposite train, the train withstands greater outward force, and when passing through the negative zone of the opposite train, the train withstands greater inward force. The lateral force on the leading car is just shown in Fig. 14b. Without the asymmetric effects caused by tunnel walls, the lateral force on train is close to zero before the trains pass by each other. In addition, the maximum amplitude of the lateral force in the present case is smaller than that in the above case, only 50% of its amplitude.

The pressure histories of two test points on the inner and outer sides at different speeds are given in Fig. 16.

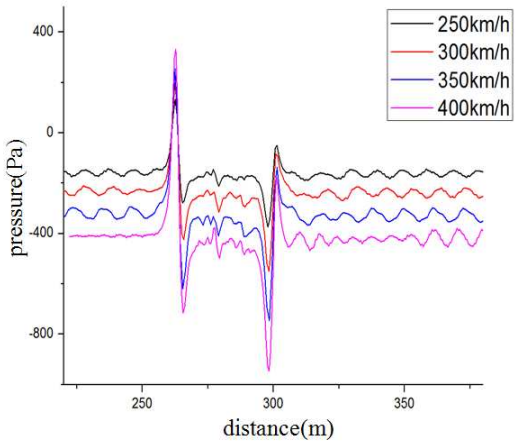

(a) Pressure variation at inner test point under different speeds

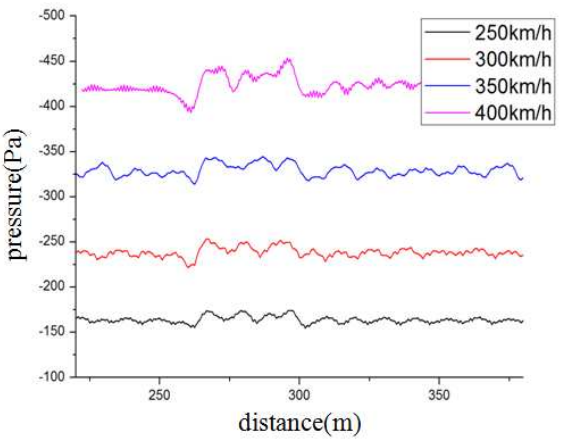

(b) Pressure variation at outer test point under different speeds

Fig.16 Pressure variation of test points under different speeds.

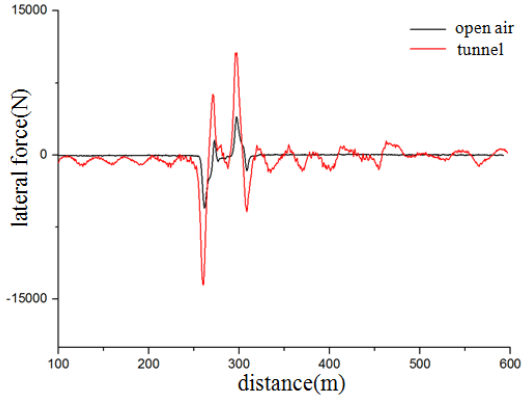

(a) Comparison of lateral force under different scenarios

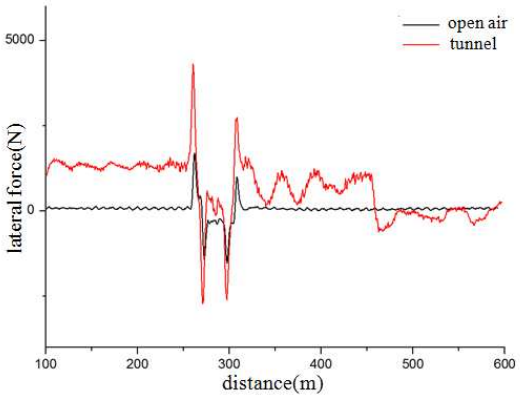

(b) Comparison of overturning moment under different scenarios

Fig.17 Comparison of aerodynamic loads under different scenarios at speed of 250 km/h.

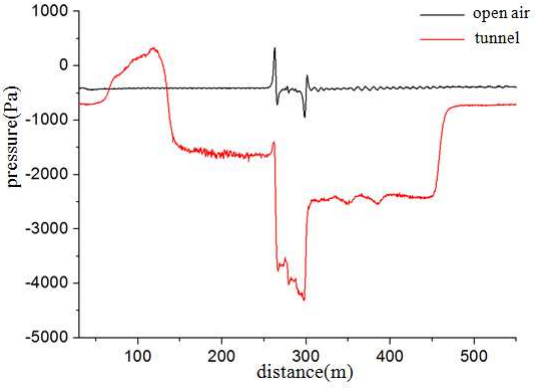

(a) Comparison of pressure variation at mh1

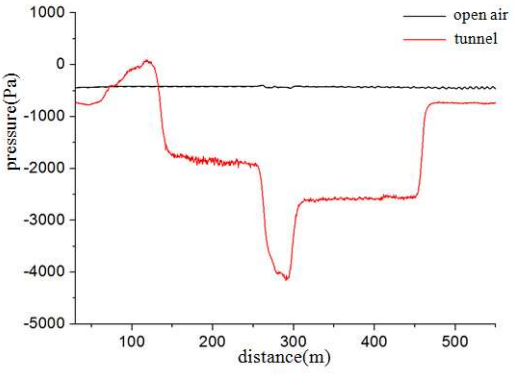

(b) Comparison of pressure variation at mh2

Fig.18 Comparison of pressure variation under different scenarios at speed of 400 km/h.

Without the tunnel compression and expansion waves, the pressure variation at the test points is simpler in form. A large pressure pulse exists when the leading and trailing noses of the opposite train pass by the test point, while the pressure is constant in other time. With the increase of the running speed, the pressure amplitude at the test points keeps increasing. But

comparing the pressure history of the inner test point with that of the outer test point, it can be observed that the pressure wave has greater influence on the inner side than the outer side. Although some fluctuations of the pressure wave on the outer side could be seen, they are far fewer than those of the pressure wave in the inner side.

By analysis of pressure at all test points on the surface of the train, the pressure extremums are approximately +233.2Pa/-373.66Pa at the speed of 250km/h, and the corresponding values are approximately +608.28Pa/-945.87Pa at the speed of 400km/h, which are 261%/253% of the extremums at the speed of 250km/h. It can be seen that the pressure wave generated by trains passing by each other in the open air is closely related to the running speed. As the speed increases, the pressure wave has significant change in the extremums. Relationships between the pressure extremums and the running speed could be obtained through numerical fitting: $P_{max} = 0.04082V_{train}^{2.0417}$ and $P_{min} = -0.1035V_{train}^{1.938}$, with correlation coefficient of 0.996 and 0.998, respectively. It can be seen that the pressure extremums are proportional to the square of the speed. In fact, the train is in the self-analog state at the running speed of 250km/h～400km/h, and the pressure coefficient $C_p = \frac{P}{0.5\rho V^2}$ in the train flow field is basically independent of the speed. Therefore, the pressure wave amplitude of the trains passing by each other is basically proportional to the square of the speed.

4.2.3 Comparative analysis of two scenarios

First the comparison of the amplitude of the aerodynamic loads in the two scenarios is performed. Fig.17 shows the amplitudes of the lateral force and overturning moment on the leading car at the speed of 250km/h. It can be seen that the amplitude of lateral force is 59773.0N and the amplitude of overturning moment is 16504.9 N·m in the condition that trains pass by each other in a tunnel. However, in the condition that trains pass by each other in the open air, the amplitudes are 24261.2N and 8063.9 N·m, respectively, which are 40.55% and 48.85% of those of the former.

This means the trains experience more severe aerodynamic loads when passing by each other in a tunnel due to the compression waves and expansion waves, and this will bring greater threat to the safe running of the trains.

Then the pressure histories at the test points in the two scenarios are analyzed. When trains pass by each other in the open air, the surface pressure of the train distributes in a sequence, namely "high pressure zone -- low pressure zone -- steady pressure zone -- sub-high-pressure zone -- sub-low-pressure zone". This will affect the aerodynamic loads of the opposite train. However, the air flow is blocked by the tunnel walls when trains pass by each other in the tunnel. Compression waves will be produced when the front of the train is running into the tunnel and expansion wave will be produced when the rear is running into the tunnel. The pressure in the tunnel will be changed during the propagation of the pressure waves, and multiple reflections at the ends of the tunnel make the pressure of the tunnel and the surface of the train more complex. Fig.18 shows the pressure comparison at the test points between two scenarios at the running speed of 400km/h.

It can be seen from Fig. 18 that pressure variation in the case of the tunnel is much stronger than that in the open air. Taking mh1 as an example, the pressure amplitude in the case of the tunnel reaches 4654.7Pa at the running speed of 400km/h, but the amplitude in the case of the open air is 1391.9Pa, just 29.9% of the amplitude of the former.

4.3 Multi-body response analysis

After obtaining the aerodynamic forces and torques of each car by CFD calculations, the coordinate is transformed to get the aerodynamic loads based on the centroid of each car. Then these quantities are loaded to the multi-body model for multi-body dynamic analysis, which focuses on the comparison of the derailment coefficient, the wheel unloading rate, the wheel/rail lateral force, and the wheel/rail vertical force. The derailment coefficient is used to evaluate whether the rim of the wheel would climb the track surface and lead to derailment. It is defined as the ratio of the lateral force to the vertical force acting on the wheel. In order to keep the train safe, this value should be less than 0.8. The wheel unloading rate is defined as the ratio of wheel load reduction to net wheel weight. It will cause derailment when the wheel unloading rate is excessive, so the safety standard is also less than 0.8. Large wheel/rail lateral force, Q, will result in track row sliding, thus a limit of this variable is defined as $Q \leq 0.85(10+P_o / 3) = 43KN$.

Large wheel/rail vertical force P may damage the track fasteners and sleepers, and even endanger

Table 2 Simulation results of derailment coefficient.

	Wheelset No.1		Wheelset No.2		Wheelset No.3		Wheelset No.4	
	left	right	left	right	left	right	left	right
Leading car	0.0697	0.0642	0.0680	0.0638	0.0682	0.0672	0.0820	0.0823
Middle car	0.0618	0.0630	0.0615	0.0610	0.0623	0.0634	0.0629	0.0619
Trailing car	0.0642	0.0640	0.0649	0.0691	0.0680	0.0659	0.0684	0.0628

Table 3 Simulation results of wheel unloading rate.

	Wheelset No.1	Wheelset No.2	Wheelset No.3	Wheelset No.4
Leading car	0.1543	0.1512	0.1536	0.1647
Middle car	0.1310	0.1281	0.1341	0.1358
Trailing car	0.1469	0.1467	0.1524	0.1495

Table 4 Simulation results of wheel/rail lateral force (N).

	Wheelset No.1		Wheelset No.2		Wheelset No.3		Wheelset No.4	
	left	right	left	right	left	right	left	right
Leading car	4600.47	4234.85	4487.36	4180.97	4607.43	4322.20	5608.62	5573.55
Middle car	3939.63	4012.59	3917.41	3849.10	4018.57	3867.22	4077.14	3962.19
Trailing car	4193.87	4205.98	4249.23	4527.29	4513.52	4102.08	4541.37	4053.88

Table 5 Simulation results of wheel/rail vertical force (N).

	Wheelset No.1		Wheelset No.2		Wheelset No.3		Wheelset No.4	
	left	right	left	right	left	right	left	right
Leading car	79550.3	79072.9	79524.0	79206.8	81409.0	81040.3	81711.1	81651.4
Middle car	75652.8	75172.9	75761.0	74998.2	76491.1	76214.6	76758.9	76556.3
Trailing car	79021.1	78642.6	78871.4	78658.8	79159.8	78450.1	79236.1	78266.8

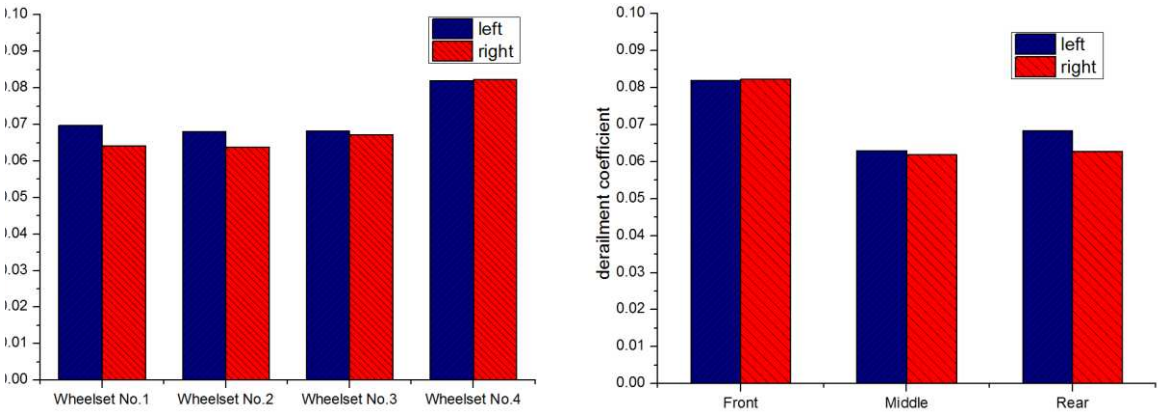

(a) Comparison of derailment coefficient of each wheelset of leading car

(b) Comparison of fourth wheelset of each car

Fig.19 Comparison of derailment coefficient.

traffic safety, so $P \leq 170\text{kN}$ is usually regarded as the safety standard.

4.3.1 Trains passing by each other in tunnel

The variation of aerodynamic loads will affect train dynamics performance. The results at the running speed of 250 km/h are taken as an example for the analysis as follows. Tables 2 – 5 show the simulation results of the above four variables of all the wheels at the speed of 250 km/h.

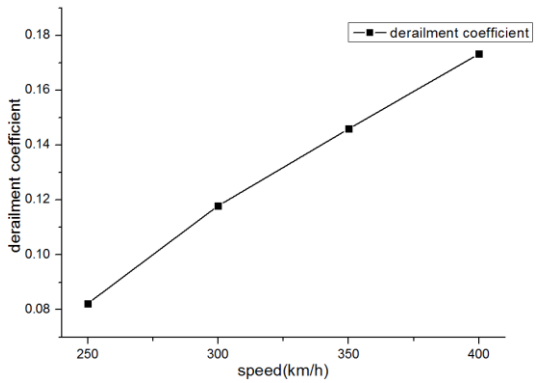

(a) Derailment coefficient

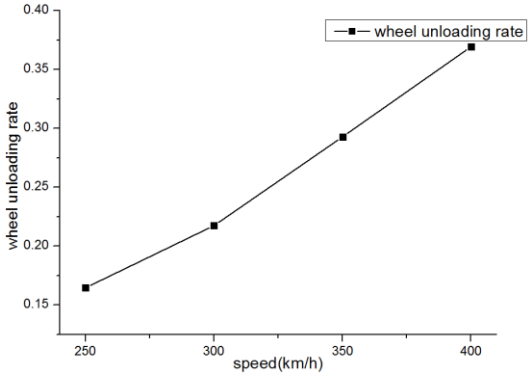

(b) Wheel unloading rate

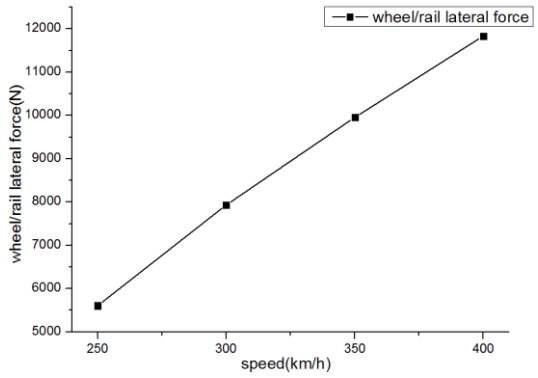

(c) Wheel/rail lateral force

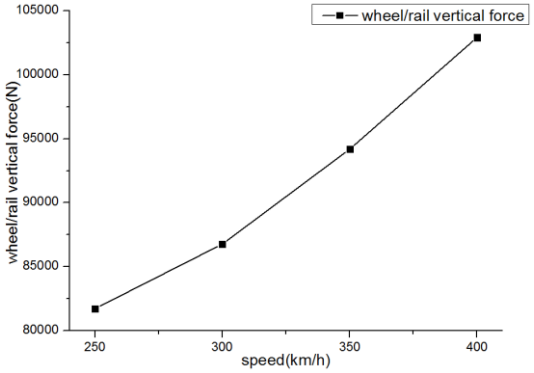

(d) Wheel/rail vertical force

Fig. 20 Variations of four assessment variables with speed for trains passing by each other in tunnel.

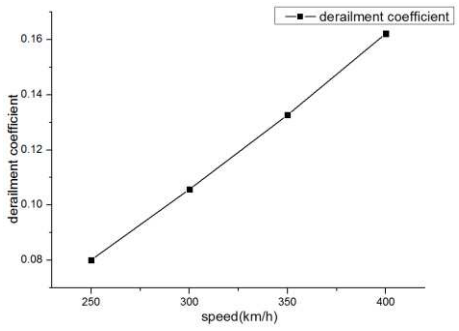

(a) Derailment coefficient

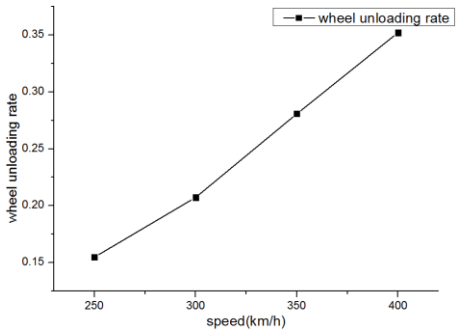

(b) Wheel unloading rate

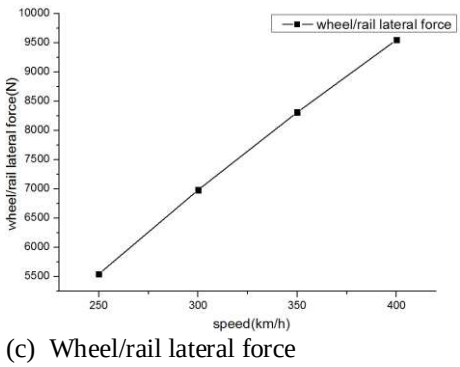

(c) Wheel/rail lateral force

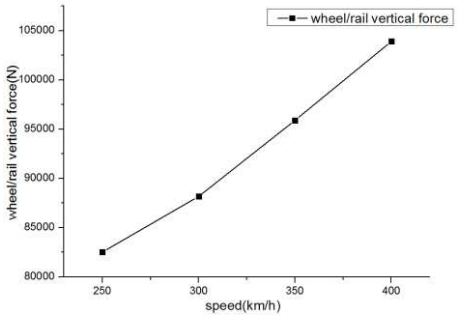

(d) Wheel/rail vertical force

Fig.21 Variations of four assessment variables with speed for trains passing by each other in open air.

Table 6 Simulation results of derailment coefficient.

	Wheelset No.1		Wheelset No.2		Wheelset No.3		Wheelset No.4	
	left	right	left	right	left	right	left	right
Leading car	0.0658	0.0670	0.0619	0.0643	0.0637	0.0650	0.0797	0.0801
Middle car	0.0617	0.0629	0.0605	0.0603	0.0607	0.0648	0.0614	0.0625
Trailing car	0.0622	0.0623	0.0593	0.0622	0.0628	0.0696	0.0648	0.0634

Table 7 Simulation results of wheel unloading rate.

	Wheelset No.1	Wheelset No.2	Wheelset No.3	Wheelset No.4
Leading car	0.1479	0.1445	0.1455	0.1548
Middle car	0.1278	0.1251	0.1284	0.1307
Trailing car	0.1473	0.1445	0.1506	0.1475

Table 8 Simulation results of wheel/rail lateral force (N).

	Wheelset No.1		Wheelset No.2		Wheelset No.3		Wheelset No.4	
	left	right	left	right	left	Right	left	right
Leading car	4333.35	4406.53	4069.89	4222.84	4407.70	4249.47	5531.19	5542.09
Middle car	3947.14	4030.63	3874.10	3833.24	3904.92	3927.97	3962.86	4002.25
Trailing car	4087.69	4129.82	3881.18	4106.55	4128.04	4285.99	4268.45	4121.65

Table 9 Simulation results of wheel/rail vertical force (N).

	Wheelset No.1		Wheelset No.2		Wheelset No.3		Wheelset No.4	
	left	right	left	right	left	right	left	right
Leading car	79276.6	78808.3	79197.8	78994.9	82163.8	81818.7	82530.0	82348.0
Middle car	75799.3	75430.5	75952.5	75294.4	76253.7	76083.6	76515.1	76382.9
Trailing car	78824.1	78935.0	78536.3	78879.5	78627.0	78436.7	78730.2	78324.3

Although the values of these four variables vary greatly from each other, they are common on the distribution. Taking the derailment coefficient as an example, Fig. 19a shows comparison of the derailment coefficient of each wheelset of the leading car, and Fig. 19b shows the comparison of the fourth wheelset of each car.

As shown in Fig. 19a, the maximum derailment coefficient of the leading car exists at the fourth wheelset. By comparing the derailment coefficient at the fourth wheelset of different cars, it can be seen that the maximum occurs in the leading car, while the middle car has the best performance. Other variables also have similar distributions. The data in the tables show that the maximum derailment coefficient exists at the fourth wheelset of the leading car, and its value is 0.0823. The maximum derailment coefficients of the middle car and the trailing car are 0.0634 and 0.0691, respectively. The maximum wheel unloading rate also occurs at the fourth wheelset of the leading car, and its value is 0.1647. The maximum wheel unloading rates of the middle car and the trailing car are 0.1358 and 0.1524, respectively. The maximum wheel/rail lateral force also exists at the fourth wheelset of the head car, and its value is 5608.62N. The maximum wheel/rail lateral forces on the middle car and the trailing car are 4077.14N and 4541.37N, respectively. The maximal wheel/rail vertical force exists at the fourth wheelset of the leading car, and its value is 81711.1N. The maximum wheel/rail vertical forces on the middle car and the trailing car are 76758.9N and 79236.1N, respectively. The data above show that the leading car has the minimum safety, followed by the trailing car, and the middle car is relatively safer.

At a fixed speed, the fourth wheelset of the leading car is the most dangerous when the high speed trains pass by each other in a tunnel. So in the following analysis this wheelset will be chosen to study the system response at different speeds. Fig. 20 shows the variation of the four variables with speed.

It can be seen that as the speed increases, the values of these four variables are all significantly increased, and the safety of the train is gradually

reduced. However, compared to their limits specified in the above, these variables are still in a safe range. This means the train operation is still safe when the high speed trains pass by each other in a tunnel in the speed range of 250km /h~400km/h. This is mainly because the time of passing by each other is quite short, and even though more severe aerodynamic loads occur during this short time, they will not immediately affect the safety of the train.

In addition, certain linear relationships could be detected between the four variables and the speeds. After performing linear fitting to each variable, the derailment coefficient approximately satisfies $Q/P = -0.06584 + 0.0006022 \times V_{train}$, and its correlation coefficient is 0.994; the wheel unloading rate approximately satisfies $\Delta P/P = -0.186 + 0.00138 \times V_{train}$, and its correlation coefficient is 0.99; the wheel/rail lateral force approximately satisfies $Q = -4624.082 + 41.40826 \times V_{train}$, and its correlation coefficient is 0.996; the wheel/rail vertical force approximately satisfies $P = 45211.39 + 142.1078 \times V_{train}$, and its correlation coefficient is 0.98. Based on the linear relationships of the assessment variables with speed, it can be obtained that the limit of the running speed when trains pass by each other in a tunnel is about 714km/h in accordance with the limits of the four variables.

4.3.2 Trains passing by each other in open air

Excited by aerodynamic loads, dynamic performance of the train deteriorates when the high speed trains pass by each other. Numerical results at the running speed of 250km/h are taken as an example to analyze the four variables of the leading, middle and trailing cars. Simulation results are shown in Tables 6-9.

The derailment coefficient has a maximum at the fourth wheelset of the leading car, and so do the other three assessment variables. The maximum derailment coefficient is 0.0801, and the maximum derailment coefficient of the middle and trailing car are 0.0648 and 0.0696, respectively. The maximum wheel unloading rate is 0.1548, and the maximum wheel unloading rates of the middle car and the trail car are 0.1307 and 0.1506 respectively. The maximum wheel/rail lateral force is 5542.09N, and the maximum wheel/rail lateral forces on the middle car and the trail car are 4030.63N and 4285.99N, respectively. The maximum wheel/rail vertical force is 82530N, and the maximum wheel/rail vertical forces on the middle car and the trail car are 76515.1N and 78935N, respectively. It can be concluded that response characteristics of the aerodynamic loads are the same as those case in a tunnel, that is, the leading car is the most dangerous, followed by the trailing car, and the middle car is relatively safer.

It can be seen that the fourth wheel set of the leading car has the worst dynamic performance. So it is chosen to study the response characteristics at different speeds. Fig.21 shows the variations of the four assessment variables with speed.

It can be seen that as the speed increases, the values of the derailment coefficient, the wheel unloading rate, the wheel/rail lateral force and the wheel/rail vertical force are all significantly increased, and the train safety is gradually reduced. When the trains run at a speed of 400km/h, the derailment coefficient, the wheel unloading rate, the wheel/rail lateral force and the wheel/rail vertical force are 0.1622, 0.3521, 9552.64N, 103906.9N, respectively. In accordance with the limits of the four assessment variables, all values satisfy the conditions of safe operation. This means the train operation is still safe when the high speed trains pass by each other in the open air with the speed range of 250km/h~400km/h.

It could be observed that linear relationships exist between the assessment variables and the running speed of the train. After linear fitting, the derailment coefficient approximately satisfies $Q/P = -0.05747 + 0.0005466 \times V_{train}$, and its correlation coefficient is 0.998; the wheel unloading rate approximately satisfies $\Delta P/P = -0.18 + 0.00133 \times V_{train}$, and its correlation coefficient is 0.992; the wheel/rail lateral force approximately satisfies $Q = -1088.266 + 26.72398 \times V_{train}$, and its correlation coefficient is 0.998; the wheel/rail vertical force approximately satisfies $P = 45916.25 + 143.718 \times V_{train}$, and its correlation coefficient is 0.991. Based on the linear relationships of the assessment variables with speed above, it can be obtained that the limiting speed when trains pass by each other in the open air is about 737km/h in accordance with the limits of the four assessment variables.

4.3.3 Comparative analysis

Finally comparative analysis of dynamic performance in two scenarios at different speeds is performed as shown in Fig. 22.

As seen in Fig. 22, the values of the derailment coefficient, the wheel unloading rate and the wheel/rail lateral force on the trains passing by each other in the open air are slightly

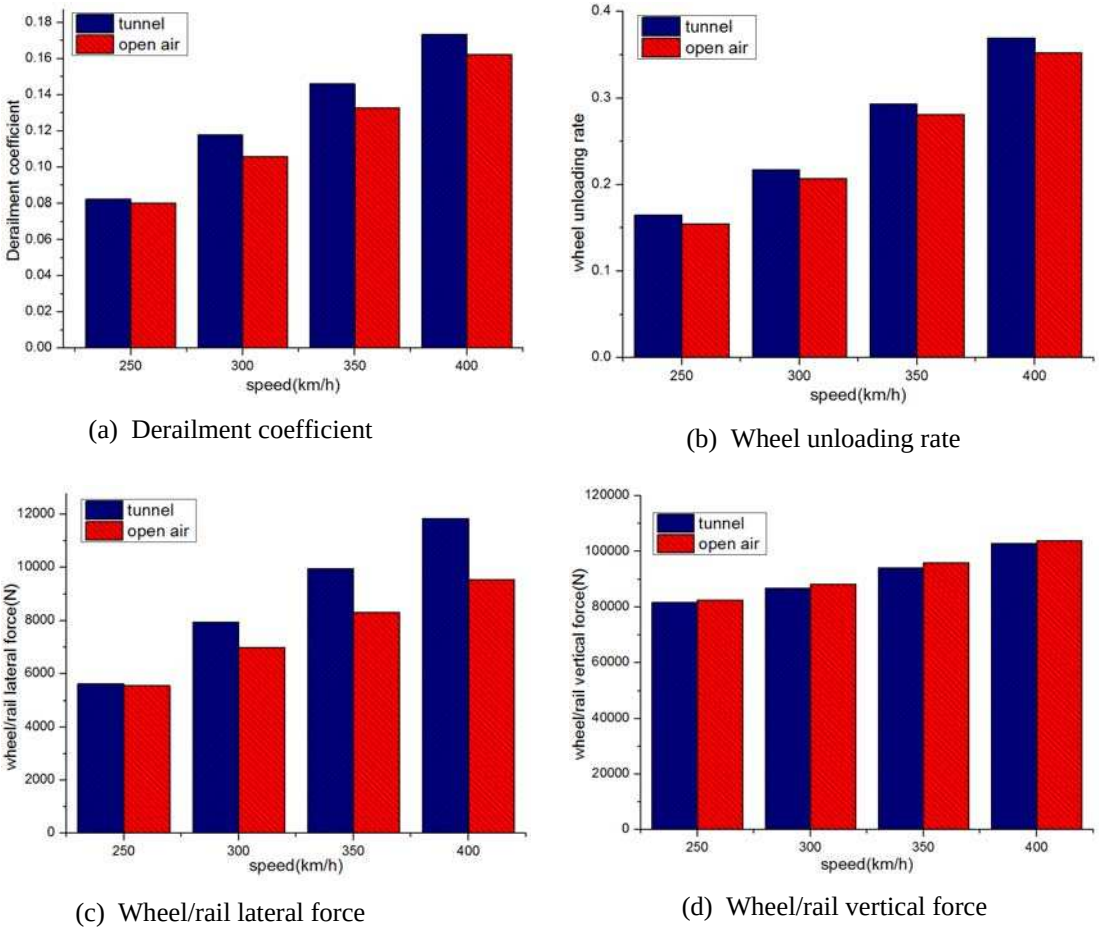

(a) Derailment coefficient

(b) Wheel unloading rate

(c) Wheel/rail lateral force

(d) Wheel/rail vertical force

Fig.22 Comparison of four assessment variables between different scenarios.

lower than those of the case in a tunnel, although the value of the wheel/rail vertical force is slightly bigger. Thereby, the train safety in the case of the tunnel is worse than that of the case in the open air due to the tunnel pressure waves. No matter what the scenario is, the values of the four variables are much lower than their limits. The approximate linear fitting is performed for the four assessment variables. Comparing the limit speeds of the two scenarios obtained by linear fitting, the safety of trains passing by each other in a tunnel is slightly worse than that of the case in the open air. Considering that the correlation coefficient in the tunnel case (the minimum correlation coefficient is 0.98) is a little lower, the actual speed limit should be lower than the result obtained in the present paper. In all the cases considered in the present paper, both scenarios all satisfy the safe running requirements.

5. CONCLUDING REMARKS

In the present paper, unsteady aerodynamic performance of the three-carriage CRH3 high speed trains passing by each other in a tunnel and in the open air has been firstly analyzed with the use of the moving mesh technique. In order to predict the aerodynamic performance more accurately, the computational model takes most auxiliary components into consideration, with the bogies, windshields, pantograph shrouds and air conditioner shrouds included. Unsteady aerodynamic loads obtained by the simulation are loaded on the multi-body model of three-carriage CRH3 high speed train and the analysis of multi-body system response characteristics in two scenarios has been performed. By comparing the derailment coefficient, the wheel unloading rate, the wheel/rail lateral force and the wheel/rail vertical force, the train safety has been discussed, and the variations of the four assessment variables with the train running speed has been summarized.

The variation of drag and lateral force are significantly affected by the pressure distribution on the streamline of the leading and trailing cars of the opposite train. Strong fluctuations of drag and lateral force could be triggered when the leading and trailing streamlines of the opposite train pass by.

Aerodynamic loads of the case in a tunnel are obviously larger than those of the case in the open air. The extremums of lateral force, drag and overturning moment of the latter are only half of those of the former, or even lower. The drag characteristics of the case in a tunnel are significantly different from those of the case in the open air. Due to the constraint of the tunnel wall, the sudden drop of the airflow area causes the increase of the velocity of the airflow around the train at the passing by moment. Furthermore, the surface pressure and aerodynamic drag of the train are suddenly reduced, and the amplitude of drag is even lower than that of the case in the open air.

The surface pressure of the train is severely influenced by the tunnel compression waves, expansion waves and the variation of the circulation space when trains pass by each other in the tunnel. The pressure variation with time is more complex than that of the case in the open air. In both scenarios the relationship between the pressure extremums and the square of the running speed is approximately linear.

The fourth wheelset of the leading car is the most dangerous position in both scenarios. The leading car has the worst safety, followed by the trailing car, and the middle car owns the best safety. By analyzing the derailment coefficient, the wheel unloading rate, the wheel/rail lateral force and the wheel/rail vertical force, it can be known that these four assessment variables of both cases are all within the safe operation limits, indicating that the train could safely run under the two scenarios at the speeds considered in the present paper. Worse aerodynamic loads exist when trains pass by each other in the tunnel, resulting in a worse running scenario. Linear relationships exist between the four assessment variables of the fourth wheelset and the running speeds.

ACKNOWLEGDEMENTS

This work was supported by the Major State Basic Research Development Program of China ("973" Program) (Grant No. 2011CB711100) and National Key Technology R&D Program (Grant No. 2009BAQG12A03).

REFERENCES

1. Baker C (2010). The flow around high speed trains. Journal of Wind Engineering and Industrial Aerodynamics 98(6-7): 277-298.
2. Baker C, Hemida H, Iwnicki S, Xie G, Ongaro D (2011). Integration of crosswind forces into train dynamic modeling. Proceedings of the Institution of Mechanical Engineers Part F: Journal of Rail and Rapid Transit, 225(2): 154-164.
3. Fluent Inc. FLUENT 6.3 User's Guide [EB/OL]. http://www.fluent.com.
4. Hemida H, Krajnovic S (2008). LES study of the influence of a train-nose shape on the flow structures under cross-wind conditions. Journal of Fluid Engineering 130(9):1-12.
5. Hemida H, Krajnovic S (2010). LES study of the influence of the nose shape and yaw angles on flow structures around trains. Journal of Wind Engineering and Industrial Aerodynamics 98(1):34-46.
6. Hussain A, Reynolds WC (1970). The mechanics of an organized wave in turbulent shear flow. Journal of Fluid Mechanics 41(2): 241-258.
7. Hwang J, Lee DH, Lee SG (2001). Numerical study of unsteady flow field around high speed trains passing by each other. JSME International Journal Series B 44(3): 451-464.
8. Katsuhiro K, Tatsuo M, Mitsunori Y (1996). Numerical simulation of the phenomena due to the passing by of two bodies using the unsteady boundary element method. International Journal for Numerical Methods in Fluids 23(5): 445- 454.
9. Liang XF, Tian HQ (2002). Test research on crossing air pressure pulse of 200 km/h electric multiple unit. Journal of Central South University of Technology (Natural Science) 33(6) : 621- 624 (in Chinese).
10. Mao J，Ma XJ，Xi YH (2011). Research on the running stability of high-speed trains under the cross wind by means of simulation. Journal of Beijing Jiaotong University 35(1):44-53 (in Chinese).
11. Nishino T, Roberts GT, Zhang X (2008). Unsteady RANS and detached-eddy simulations of flow around a circular cylinder in ground effect, Journal of Fluids and Structures 24(1): 18-33.
12. Pierre P, Arturo B, Paolo M (2007). Nature of pressure waves induced by a high-speed train travelling through a tunnel. Journal of Wind Engineering and Industrial Aerodynamics 95(8):781-808.
13. Raghuathan S， Kim HD, Setoguchi T (2002). Aerodynamics of high-speed railway train. Progress in Aerospace Sciences 8(6): 469-514.
14. Robert AM, Samuel H, Lee HS (2002). Measurement of the aerodynamic pressures produced by passing trains. Proceedings of the 2002 ASME/IEEE Joint Rail Conference, Washington DC, USA, 57-64.
15. Sanjay R (1994). Unsteady flow simulations using unstructured sliding meshes. AIAA-94-2333.
16. Shih TH , Liou WW, Shabbir A, Yang ZG, Zhu J (1995). A new k-ϵ eddy viscosity model for high Reynolds number turbulent flows. Computers& Fluids 24(3):227-298.
17. Spalart PR (2000). Strategies for turbulence modeling and simulations, International

Journal of Heat and Fluid Flow 21(3):252–263.
18. Tian HQ (2009). Formation mechanism of aerodynamic drag of high-speed train and some reduction measures. Journal of Central South University of Technolog 16: 166-171.